Journal of Materials Chemistry C

Accepted Manuscript

This article can be cited before page numbers have been issued, to do this please use: J. Yi, L. Zhao, W. Xu, C. Liu, W. Lai and W. Huang, *J. Mater. Chem. C*, 2016, DOI: 10.1039/C6TC01606E.

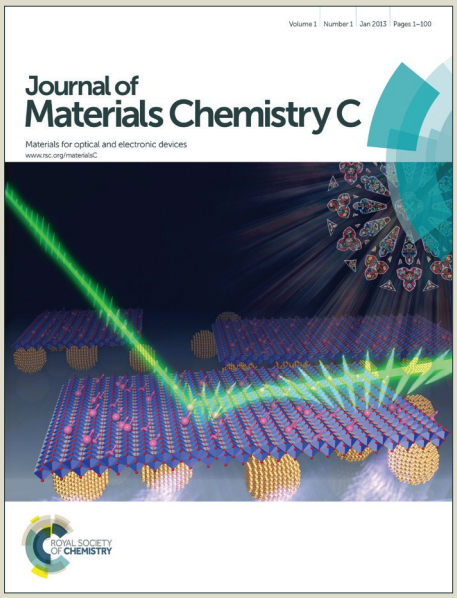

ROYAL SOCIETY OF CHEMISTRY

www.rsc.org/materialsC

View Article Online
DOI: 10.1039/C6TC01606E

Journal Name

ARTICLE

Pyrene-Capped Starburst Emitters as Gain Media for Organic Lasers: Design, Synthesis, and Stabilized Lasing Properties‡

Received 00th January 20xx,
Accepted 00th January 20xx

DOI: 10.1039/x0xx00000x

www.rsc.org/

Jian-Peng Yi,[a,†] Li Zhao,[a,†] Wei-Dong Xu,[a] Cheng-Fang Liu,[a] Wen-Yong Lai,*[a,b] Wei Huang[a,b]

A set of pyrene-capped starburst orgainc emitters composed of a non-planar cross-shaped spirofluorene core (SF-PyF) and a large rigid planar pyrene core (Py-PyF) have been designed, synthesized and explored as efficient emitters for organic lasers. High photoluminescence yields, excellent thermal stability of SF-PyF and Py-PyF in neat films make them promising optical gain media. Low amplified spontaneous emission (ASE) thresholds of 6.6 μJ/cm² (1.3 kW/cm^2) at 451 nm for SF-PyF and 5.4 μJ/cm² (1.1 kW/cm^2) at 490 nm for Py-PyF, were obtained (pump pulse: λ_p = 355 nm, 10 Hz, 5 ns). Distributed feedback (DFB) lasers based on SF-PyF and Py-PyF exhibited good performance with low thresholds (16 nJ/pulse for SF-PyF and 24 nJ/pulse for Py-PyF, respectively) and the full width at half maximum of about 0.2 nm. Surprisingly, DFB lasers integrated with SF-PyF and Py-PyF as gain media exhibited excellent ambient photostability and superior reliability even in hot water (80 °C). The excellent stability of ASE spectra, electroluminescence spectra and lasing spectra under harsh conditions manifests that the resulting pyrene-capped starburst emitters are beneficial for improving the lasing stability issues. The study sheds light on exploring robust organic gain media toward electrically-pumped OSLs.

Introduction

Organic semiconductors have found various applications in optoelectronic devices, such as organic light-emitting diodes (OLEDs), organic field-effect transistors (OFETs) and organic photovoltaic cells (OPVs).[1-4] A particularly challenging application is as gain media for organic semiconductor lasers (OSLs).[5-8] OSLs possess many fascinating advantages such as flexbility, easy fabrication and tunable optoelectronic properties. Although much progress have been achieved since the first demonstration of optically-pumped organic lasing in 1996,[9] realization of the electrically-dirven OSLs still remains a worldwide challenge.[10] To realize electrically pumped organic lasing, relatively high current density (more than 1,000 A/cm^2) is one of the prerequisites for OSLs since a large number of excited states are required to generate within the gain media layer.[5] Although it can be easily obtained upon optical excitation, similarly high excitation densities under electrically-pumped conditions need high carrier mobility to facilitate fast charge transport to the recombination zone. It is thus generally not easy for OSLs to achieve the high number of excited states to realize light amplification by electrical exicitation. Much recent work has been focused on exploring novel optical gain media with large stimulated emission cross sections (σ_e), high carrier mobility, excellent power-conversion efficiencies and low lasing thresholds.[11-14]

From a practical point of view, one has to consider that high current density in organic lasing is believed to cause a lot of heat during the device operation, which will seriously affect the device performance or even destroy the device. Therefore, apart from high luminescence efficiecy, OSLs require more strict criteria to fulfill compared with OLEDs.[14] In order to ensure the lasing stability and reliability, high material stability including thermal stability, optical stability, and electrical stability are required for electrically-driven organic lasers. Currently, although increasing attention has been focused on the aspects of improving the lasing properties to address the challenge to realize electrically-driven organic lasing, successful strategies concerning the molecular design on enhancing the lasing stabiltiy are quite limited. In this context, it is desirable to develop novel materials with excellent lasing stability while maintaining good optical gain properties.

From a fundamental perspective, the molecular design is of great significance to achieve the stimulated emission properties of OSCs. Fluorene is favorably employed as an important building block due to its high photoluminescence quantum yields (PLQYs), good solubility in various solvents and excellent film-forming ability.[1,14] However, the relatively poor optical stability and the undesirable long-wavelength emission under electrical conditions have seriously impeded their practical applications in optoelectronic devices.[1,15] Various building blocks, such as pyrene, spirofluorene, porphyrin,

[a] Key Laboratory for Organic Electronics and Information Displays (KLOEID), Institute of Advanced Materials (IAM), Jiangsu National Synergetic Innovation Center for Advanced Materials (SICAM), Nanjing University of Posts & Telecommunications, 9 Wenyuan Road, Nanjing 210023, China. E-mail: iamwylai@njupt.edu.cn
[b] Key Laboratory of Flexible Electronics (KLOFE) & Institute of Advanced Materials (IAM), Jiangsu National Synergetic Innovation Center for Advanced Materials (SICAM), Nanjing Tech University (NanjingTech), 30 South Puzhu Road, Nanjing 211816, China.
† J.-P. Y. and L. Z. contributed equally to this work.
‡ Electronic Supplementary Information (ESI) available: Additional experimental methods, 1H NMR and MALDI-TOF spectra, TGA, DSC, electrochemical properties, electroluminescent properties, and ASE spectra under various conditions. See DOI: 10.1039/x0xx00000x

View Article Online
DOI: 10.1039/C6TC01606E

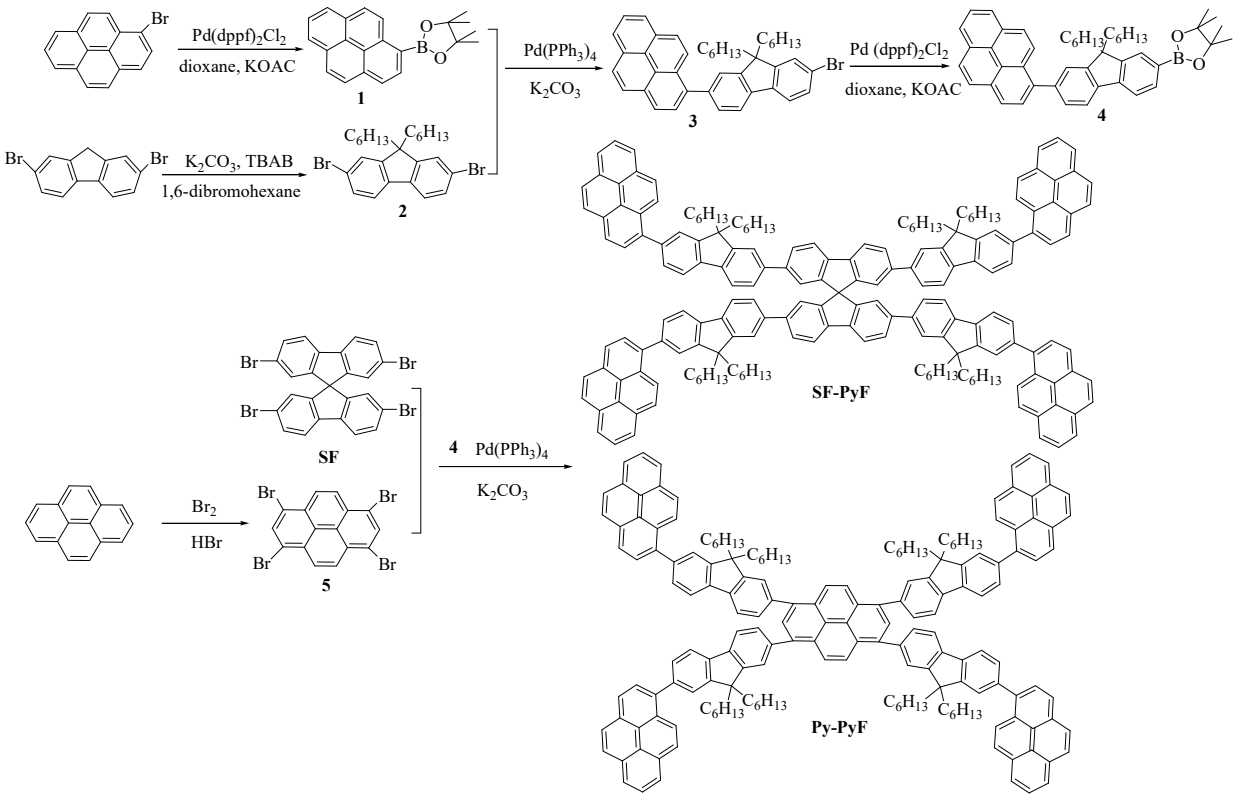

Scheme 1. Synthetic routes of SF-PyF and Py-PyF.

anthracene, and truxene have been used to construct starburst materials, resulting in attractive electroluminescence and lasing properties in this system.[8,16-22] Among these, pyrene has attracted particular interest because of high photoluminescence efficiency, high charge carrier mobility and excellent thermal stability.[23] More importantly, in comparison to fluorene derivatives with poor spectral stability, the remarkable thermal stability of pyrene molecules is promising for organic lasing applications. Nevertheless, planar pyrene derivatives are inclined to generate π aggregates/ excimers in the solid states, leading to red-shifted aggregates/ excimers emission with lower fluorescence efficiency. Following the approach of obtaining targeted optical and electrical properties by adjusting molecular structures accordingly, we have previously reported a series of monodisperse multi-armed starbursts with pyrene as the core and fluorene as the arms, manifesting excellent amplified spontaneous emission (ASE) properties with low thresholds for organic lasers.[16,17,22] Consequently, the desirable combination of features render the novel molecular architectures important as organic lasing gain media with excellent electroluminescence performance, extremely low thresholds as well as enhanced ASE stability.

In this contribution, a novel set of butterfly-shaped molecules (referred to as SF-PyF and Py-PyF, shown in Scheme 1) are designed, synthesized and explored as efficient optical gain media for organic lasers. In combination with pyrene as the end-cappers and fluorene as the bridge arm, the core structure is varied with choosing spirofluorene or pyrene as building blocks to unravel the relationships between molecular structures and optoelectronic properties. On one hand, a spirofluorene unit possessing high emissive properties and good thermal and morphological stabilities was introduced as the core for SF-PyF.[19,20] On the other hand, in the case of Py-PyF, pyrene was empolyed as the core due to its high PLQY and good thermal stability.[23] Owing to the synergetic effects of these fascinating building blocks, the resulting novel starbursts have demonstrated not only relatively good solubility in various solvents and excellent film-forming properties but also high environmental stability and high emissive properties. The morphology, thermal stability, and corresponding ASE properties are explored in detail, implying that the butterfly-shaped pyrene-capped architectures make a significant contribution to the lasing stability. In addition, the wavelength-tunable laser devices integrated with the novel materials exhibit good performance and operational stability even under water conditions. In particular, the ASE spectra, lasing spectra and electroluminescence spectra based on the molecular gain media exhibit excellent photostability under severe external conditions. Bearing these results in mind, it is believed that the novel molecular design endow the resulting materials with rather attractive characteristics such as excellent lasing stabiliy and high electroluminescence properties, holding great promise for electrically-pumped OSLs.

Results and discussion

Synthesis and characterization.

The detailed synthetic routes of the samples, SF-PyF and Py-PyF, are depicted in Scheme 1. The key steps of the synthetic procedures involved Suzuki cross-coupling reaction of pyrene-capped

View Article Online
DOI: 10.1039/C6TC01606E

oligofluorene with 2,2',7,7'-tetrabro-9,9'-spirodifluorene or 1,3,6,8-tetrabromopyrene using $Pd(PPh_3)_4$ as catalyst to yield SF-PyF and Py-PyF in 20–30% yields after heating at 95 °C for 12 h. The well-defined structures and chemical purities of the intermediates and the final starbursts were adequately verified by ^1H and ^{13}C NMR spectroscopy and MALDI-TOF mass spectrometry (Fig. S1).

Thermal stability.

Thermal properties of SF-PyF and Py-PyF were investigated by thermogravimetric analysis (TGA) and differential scanning calorimetry (DSC). As revealed by TGA in Fig. S2a, both SF-PyF and Py-PyF exhibited excellent thermal stability with their decomposition temperature (T_d) at 393 °C and 402 °C, respectively. According to DSC measurements that was repeated several times, no distinct glass transition temperature (T_g) was observed for the samples (Fig. S2b). The melting temperatures (T_m) over 280 °C were recorded for both SF-PyF and Py-PyF. The excellent thermal properties are attributed to the synergestic effects of the chemical structures with novel pyrene-capped starburst molecular design.

Photophysical properties.

Fig. 1 depicts the normalized UV-vis absorption, photoluminescence (PL), and amplified spontaneous emission (ASE) spectra of the butterfly-shaped SF-PyF (Fig. 1a) and Py-PyF (Fig. 1b) in dilute THF solutions and thin film states. The absorption spectrum of SF-PyF in the thin film is a little altered from that in THF solution, manifesting only one peak at 371 nm with the maximum absorption coefficient (α_{max}) of 13.6×10^4 cm^{-1}. As for the absorption spectra of Py-PyF in both THF and film states, the major bands of Py-PyF are observed at 360 nm with a shoulder peak at 410 nm, a characteristic absorption signal for π-extended pyrene units,[16] with α_{max} of 8.7×10^4 cm^{-1}. In the film state, the PL spectrum of SF-PyF exhibits two well-defined vibronic peaks at 433 nm (0-0) and 454 nm (0-1), and is relatively red-shifted (12 nm) from that in THF. In light of the PL spectrum of Py-PyF in film, two peaks at 485 nm (0-0) and 498 nm (0-1) are observed, and it is red-shifted (22 nm) in comparison to that in THF. It is noted that the emission of Py-PyF exhibits an obvious redshift of 35 nm compared with that of SF-PyF in films.

Distinct emission behaviors of the two emitters are close related to their different electron density distributions, as revealed by the theoretical calculations (Fig. S3). According to the calculation results, the spatial configuration of SF-PyF with a spirofluorene core turns out to be twisted with a twist angle of about 88.5°, and the HOMO and LUMO electron cloud distributions are dominated by the fluorene trimer strucuture. In contrast, the pyrene core for Py-PyF prefers a favorable planar configuration, and the electronic properties (HOMO and LUMO energy levels) are mainly determined by the central pyrene unit. Clearly, the emission of SF-PyF is essentially from the fluorene trimers and the emission of Py-PyF is dominated

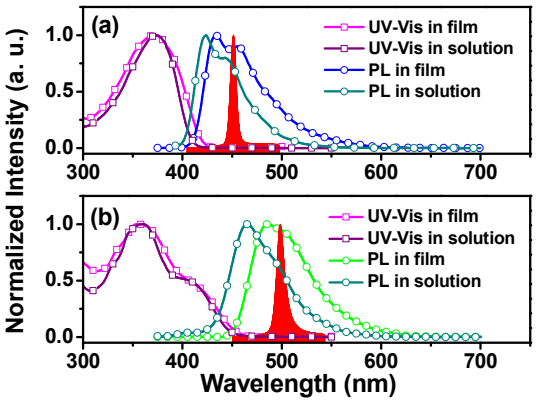

Fig. 1 Normalized UV-vis and PL spectra of (a) SF-PyF and (b) Py-PyF in dilute THF solutions and in thin films. The ASE spectra in planar waveguides recorded from films are also shown as filled curves.

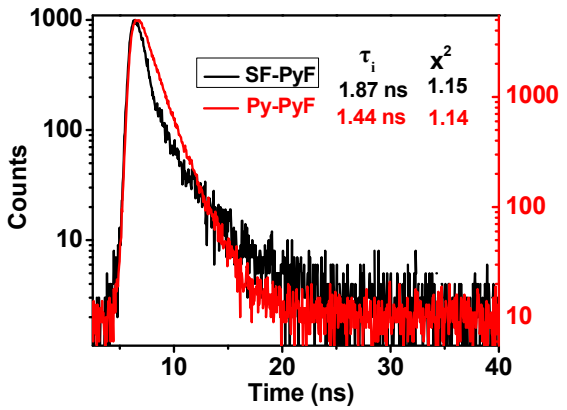

Fig. 2 Fluorescence emission decays of SF-PyF and Py-PyF in dilute THF solutions, collected at 435 and 485 nm. χ^2 are also presented.

Table 1. Photophysical properties of SF-PyF and Py-PyF

Compd	λ_{abs} [nm] (THF)[a)]	λ_{em} [nm] (THF)[a)]	λ_{abs} [nm] (film)[b)]	λ_{em} [nm] (film)[b)]	α_{max} [$\times10^4$ cm^{-1}][c)]	Φ_{PL} (THF)[a,b)]	Φ_{PL} (film)[b,c)]	Decay time [ns] (THF)[a)]	Decay time [ns] (film)[c)]	Radiative Lifetime [ns] (THF)[a,d)]
SF-PyF	374	422,443	371	434,451	13.6	0.71	0.62	0.63(45%), 2.89(55%)	0.58(58%) 2.97(42%)	2.63
Py-PyF	360	465	355,410	485,498	8.7	0.85	0.74	1.44	1.07(76%) 2.15(24%)	1.69

[a)] THF solution with concentration of 5×10^{-6} mol/L; [b)] Φ_{PL} measured with integrate sphere; [c)] prepared by spin-coating 2000 rpm from $CHCl_3$ solutions; [d)] calculated by the equation of $\tau_R = \tau/PLQY$.

View Article Online
DOI: 10.1039/C6TC01606E

by the central pyrene with an effective extended conjugation with the four attached fluorene arms.

The PL quantum yields (PLQY) and PL decays for SF-PyF and Py-PyF in dilute THF solutions and thin film states have also been measured and the data are summarized in Table 1. They were determined to be 0.71 and 0.85 for SF-PyF and Py-PyF, respectively, in dilute solutions. When going into the film states, the PLQY values of 0.62 (SF-PyF) and 0.74 (Py-PyF) still maintained quite high, suggesting efficient emissive properties in the condensed states for both the two samples. In addition, the corresponding average fluorescence lifetimes were estimated to be 1.87 ns and 1.44 ns for SF-PyF and Py-PyF, respectively, in dilute THF solutions (Fig. 2), while the radiative lifetimes are calculated to be 2.63 ns and 1.69 ns for SF-PyF and Py-PyF in films, respectively. Here, reduced χ^2 values were employed as the goodness-of-fit criteria. The values are within 1.2, which conforms that the experimental results are reliable. According to the analysis, SF-PyF had a slower decay than Py-PyF, which implied that there were stronger intermolecular interactions in the film of Py-PyF, creating more energy migration path. It is obvious that the core structure impacts the intermolecular interactions, thus modulating the photoluminescence decay behaviors in films.

Electronic and electroluminescent properties.

To get insights on the electronic properties of SF-PyF and Py-PyF, Gaussian simulation (Fig. S3) and cyclic voltammetry (CV) (Fig. S4) were carried out. The results are summarized in Table S1. By means of CV measurements, the HOMO and LUMO levels were estimated for SF-PyF (-5.86 eV, -2.33 eV) and Py-PyF (-5.74 eV, -2.32 eV), indicating *p*-type characteristics of these molecules. Optical band gaps (E_g^{opt}) of SF-PyF (2.96 eV) and Py-PyF (2.73 eV) were obtained from the absorption onsets in film states, which followed similar trends as those obtained by CV measurements and Gaussian simulation.

To investigate the electroluminescent properties and especially the spectral stability under electrical bias, solution-processed OLEDs with the configuration of ITO/PEDOT:PSS/EML/TPBi(40 nm)/LiF (0.5 nm)/Al (100 nm) were fabricated (Figure S5). SF-PyF or Py- PyF as the emitting layer (EML) was spin-coated from $CHCl_3$ solution. Devices based on 4,4′-bis-(carbazol-9-yl)biphenyl (CBP) host doped with SF-PyF or Py-PyF were also fabricated for comparision. The representative performance of the OLEDs based on Py-PyF are shown in Fig. S6. It is noted that the electroluminescence spectra of the devices are almost the same with and without the host. The results confirmed that the red-shifted emissive behaviours resulting from the aggregates/excimers of the planar pyrene units have been effectively depressed due to the bulky batterfly-shaped chemical structures, suggesting non-doped characteristics of the samples. More importantly, SF-PyF and Py-PyF neat films exhibited stabilized electroluminescence properties with no distinct spectral variation under various driving voltages from 5 V to 9 V (Fig. 3), which is an important prerequisite for organic emitters as potential gain media for applications in electrically-driven OSLs.

ASE properties.

The ASE properties of the samples were investigated. The samples were optically pumped (photoexcited using λ_p = 355 nm, 10 Hz, 5 ns pump pulse) with increasing the pump energy to determine the ASE propagation in planar waveguides. As shown in Fig. 4a and 4c, both SF-PyF and Py-PyF showed a significant increase of emission intensity and a rapid decrease of the full-width at half-maximum (FWHM) linewidth of the emission when the excitation intensity exceeds a certain value. The transition from linear to a superlinear dependence of the ASE peak intensity at the pump energy density is used as an indication of ASE threshold value. By following the method to define ASE threshold, relatively low threshold values were estimated to be 6.6 μJ/cm² (1.3 kW/cm^2) for SF-PyF film (98 nm) and 5.4 μJ/cm^2 (1.1 kW/cm^2) for Py-PyF film (66 nm) with ASE peaks at 451 nm and 491 nm, respectively. It is worth noting that the threshold value of Py-PyF is slightly lower than that of SF-PyF, and the output intensity of Py-PyF increases much faster than that of SF-PyF, which can be explained by the fact that Py-PyF has a much higher radiative relaxation rate

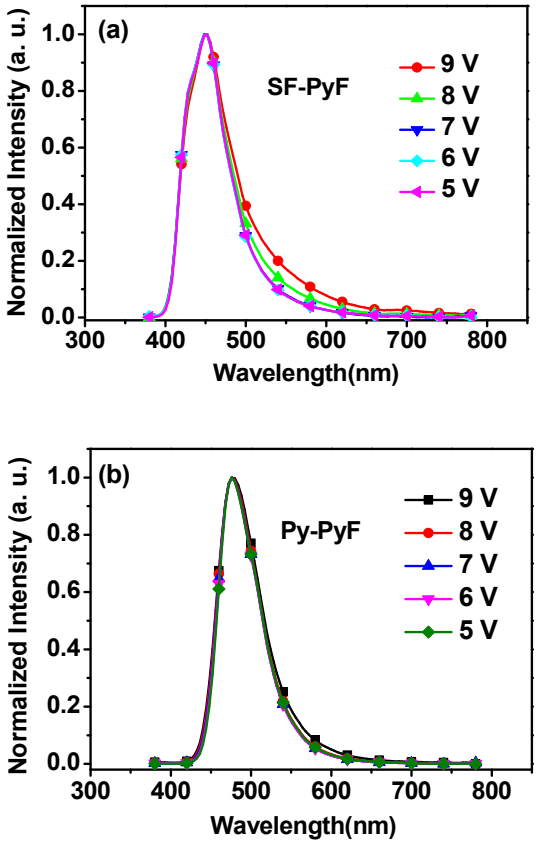

Fig. 3 Electroluminescence spectra of (a) SF-PyF and (b) Py-PyF in air at various operating voltages, with the device structure of ITO/PEDOT:PSS(40 nm)/EML(60 nm)/TPBi(40 nm)/LiF(0.5 nm)/Al (100 nm).

View Article Online
DOI: 10.1039/C6TC01606E

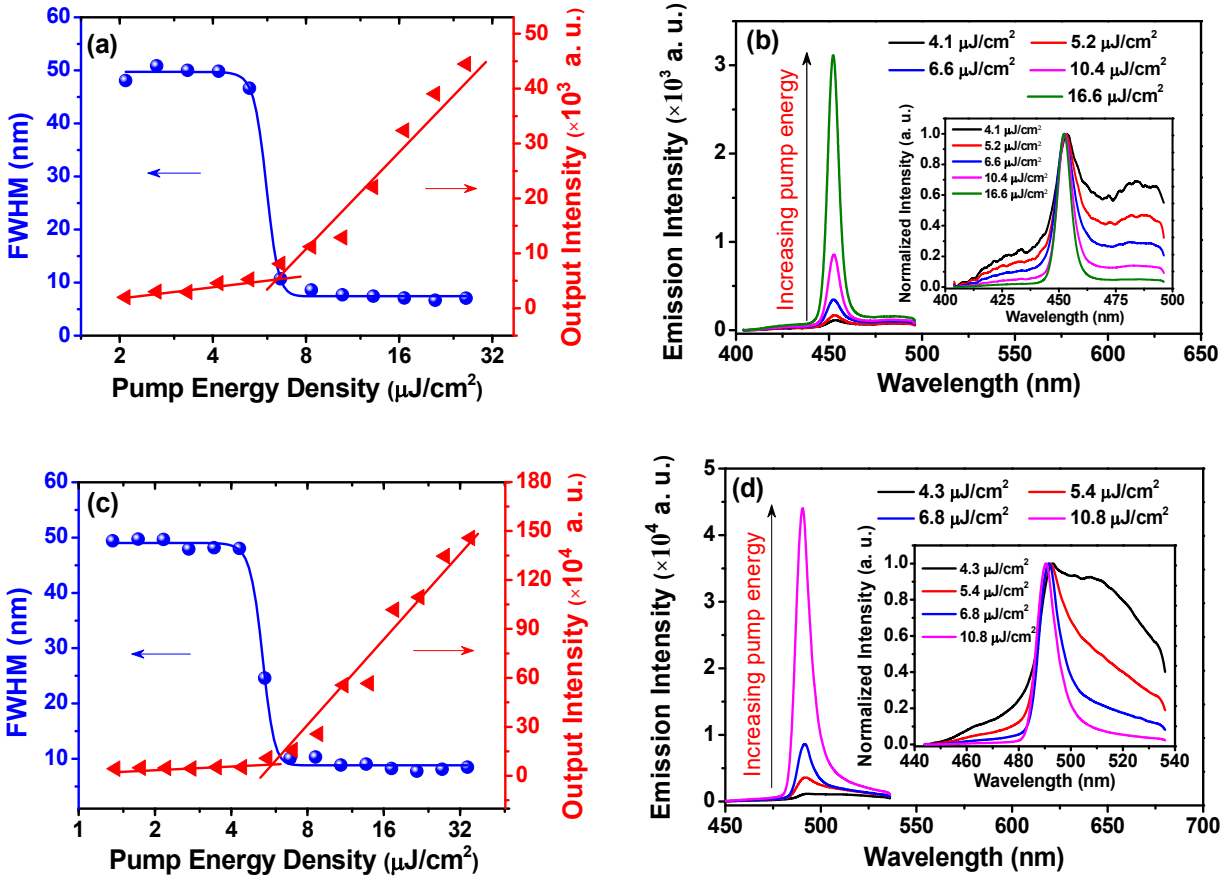

Fig. 4 Dependence of the full-width at half-maximum (FWHM, filled spheres) and the integrated output intensity (filled triangles) of the emission for (a) SF-PyF and (c) Py-PyF at various pump energy densities. The evolution of emission spectra of (b) SF-PyF and (d) Py-PyF neat films for planar waveguides with increasing the pump energy.

(3.9×10^8 s^{-1} *vs.* 5.6×10^8 s^{-1}) and better film quality as revealed later. Fig. 4b and 4d show the evolution of the emission spectra for the two slab waveguides with increasing the pump energy density. The insets depict the spectral narrowing process for both molecules as the pump fluence grows continuously. When the pump energy is at a low level, the spectra are broad with two vibronic levels. However, a sudden collapse of the linewidth is observed with the excitation fluence higher than the threshold for ASE, which can be attributed to the fact that the stimulated emission instead of spontaneous emission has become dominant in this process. The ASE spectra obtained well above the thresholds in planar waveguides are also shown in Fig. 1 as filled curves in comparison with the PL spectra. It is noted that the ASE peaks are both lying at the 0-1 vibrations, manifesting a quasi-four-level system for each sample, which is believed to be helpful for organic gain media to achieve a low threshold pumping.

Photostability

For application as gain media for electrically pumped OSLs, high stability is one of the most important prerequisites. The ASE threshold value of these materials was recorded as a function of the annealing temperature to evaluate the photostability of the thin-film samples which were maintained in air for 5 min at each annealing temperature during the test. Remarkably, the ASE thresholds remained almost the same from room temperature up to 200 °C for the starburst samples while the ASE thresholds for poly(9,9-dioctylfluorene) (PFO) showed sudden increase at 120 °C (Fig. 5a). Subsequently, the ASE threshold started to increase slightly when the films were heated up to 220 °C for SF-PyF and 240 °C for Py-PyF. The ASE phenomenon of both materials can still be detectable even if the annealing temperature increased up to 300 °C. These results indicated that the gain properties of the starburst samples were well maintained even at high temperatures. More importantly, the ASE spectra of SF-PyF kept almost the same regardless of gradually increasing the annealing temperature (Fig. S7a). In contrast, the ASE spectra of the film of PFO showed an obvious red-shift of 12 nm (from 450 nm to 462 nm) when the annealing temperature increased from 80 °C to 140 °C (Fig. S7). Upon further annealing at 160 °C, the emission spectrum of PFO film was broad and

View Article Online
DOI: 10.1039/C6TC01606E

featureless with three vibronic levels lying at around 430 nm, 448 nm and 480 nm, respectively (Fig. S7c). Meanwhile, the ASE threshold increased by 20 fold (from 8 μJ/cm^2 to 159 μJ/cm^2) upon heating at 140 °C for 5 min and the ASE was not detectable upon annealing at above 160 °C, implying a significant change of intrinsic structures for the PFO film.

Afterwards, a more harsh test was carried out to further assess the stability of the gain media. The film samples were soaked in water (80 °C) for 10 min and then blew dry by nitrogen gas carefully, and heated at 160 °C in air for 5 min, and finally cooled fast to room temperature. After the treatment, the standard ASE measurement was conducted on the samples to record the corresponding ASE actions. Cycle tests were then taken to access their stability. As shown in Fig. 5b, ASE characteristics were monitored as a function of the cycling times. The ASE thresholds for both samples showed a very slow increase by 4 fold and 2.6 fold (still at relatively low levels) after 7 cycles of tests for SF-PyF and Py-PyF, respectively. Particularly, the ASE spectra of SF-PyF (see details in Fig. S9) were almost unchanged which further confirmed a superior stability for the sample in both air and water conditions. In contrast, the ASE threshold of PFO films substantially increased from 7.7 μJ/cm^2 to 1058 μJ/cm^2 even for the first treatment cycle.

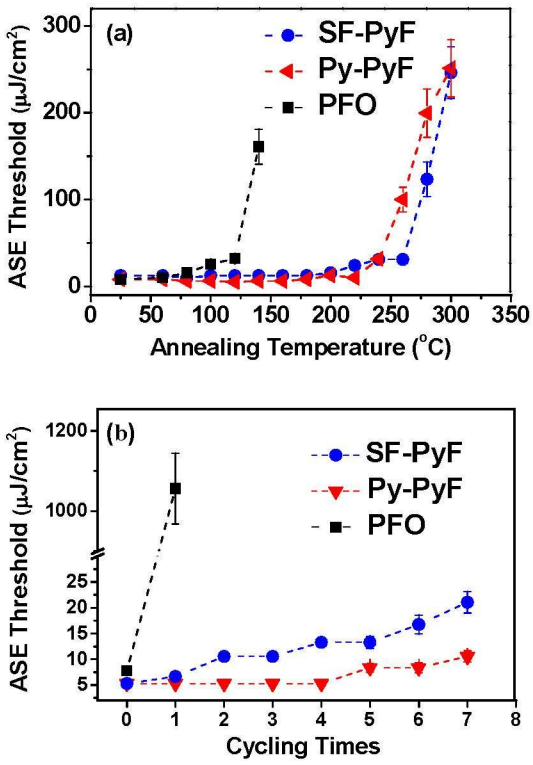

Fig. 5 Evolution of ASE threshold for SF-PyF (solid circles), Py-PyF (solid triangles) and PFO (solid squares) slab waveguides as a function of (a) annealing temperature, and (b) the treatment cycles in boiling water and annealing in air conditions.

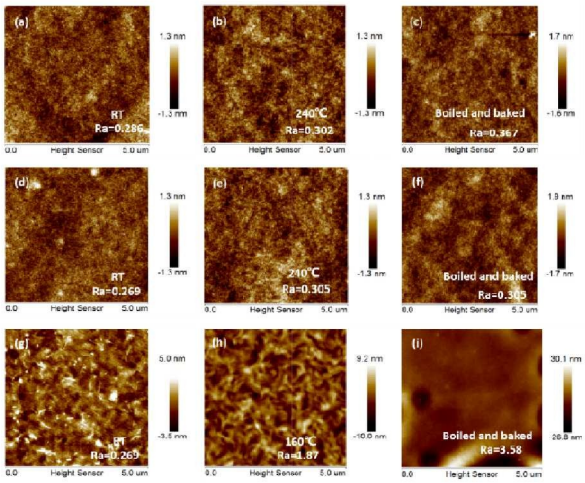

Fig. 6 AFM images of (a) (b) (c) for SF-PyF, (d) (e) (f) for Py-PyF, and (g) (h) (i) for PFO thin films under various treating conditions: room temperature (a) (d) (g); 240 °C annealed in air for 5 min (b) (d), 160 °C annealed in air for 5 min (h); boiled in water for 10 min and baked in air at 160 °C for 10 min (c) (f) (i).

Overall, SF-PyF and Py-PyF exhibit much better stability than that of PFO, suggesting excellent chemical structural stability. To understand the origin of such a distinct difference, atomic force microscope (AFM) images of SF-PyF, Py-PyF, and PFO films under various treating conditions were recorded. As shown in Fig. 6, all the samples (SF-PyF, Py-PyF and PFO) are morphologically homogeneous with relatively small mean roughness (Ra) values at room temperature. The morphologies of SF-PyF and Py-PyF remain nearly constant after annealed upon high temperature (up to 240 °C) in air. It is deduced that similar morphology stability upon heating conditions contributes to similar ASE threshold evolution trends for SF-PyF and Py-PyF waveguides (Fig. 5a). After the boiling and baking treatments, slightly increase of Ra value is observed for SF-PyF, while the roughness of Py-PyF film remians almost unchanged, indicating higher morphological stability for Py-PyF film. As a result, Py-PyF shows a slower threshold increase compared to that of SF-PyF waveguide (as shown in Fig. 5b). In contrast, PFO molecules tend to segregate in rugged structures during the thermal treatments. Furthermore, severe damages with large-sized holes were observed across over the PFO film, suggesting its hypersensitivity to the treating conditions. With poor morphological stability, PFO proved to be inadequate as stable gain media. The excellent performances of the novel pyrene-capped starburst samples, especially for Py-PyF, are thus ascribed to a combination of chemical stability and good morphological stability upon heating, which presents a compelling case as stable gain media for potential electrically-pumped OSL applications.

Lasing properties

1D gratings were fabricated by nanoimprint lithography (NIL) of low-cost, large-area nanopatterning and relatively good repetition.[27] The 2nd order gratings (50% fill factor) consisted of arrays of lines with a periodicity of 280 nm, 290 nm, and 300

View Article Online
DOI: 10.1039/C6TC01606E

nm, respectively. The modulation depth used here were 31±1 nm, much less than that of the gratings fabricated by electron-beam (e-beam) lithography. To generate SF-PyF and Py-PyF lasing, the two materials with relatively low ASE thresholds were deposited on DFB gratings by spin-coating to form laser devices, which were optically pumped using a pulsed Nd^{3+}:YAG laser (λ = 355 nm, τ = 5 ns, f_{rep} = 10 Hz) at room temperature. In order to investigte the lasing performance of the prepared DFB lasers, we studied the lasing output intensity from the organic lasers detectd by using a spectrometer upon various pump energy, to determine the lasing thresholds for both devices. As shown in Fig. 7a and 7b, with incresing the excitation fluence, a change in the slope of the output intensity was observed for each device, which denoted the thresholds of the DFB lasers. The minimum lasing threshold measured for SF-PyF (123 nm) laser was 0.77 kW/cm^2 (16 nJ/pulse) at 468 nm with a grating period of 290 nm. A low threshold value of 1.2 kW/cm^2 (24 nJ/pulse) at 481 nm was obtained for Py-PyF (150 nm) laser with a grating period of 290 nm. Above the lasing thresholds, the surface-emission spectra based on the DFB resonators for both devices narrowed into one peak with the full width at half maximum (FWHM) of around 0.2 nm. Follwing the principle of tuning the lasing peaks by means of regulating periods of DFB gratings and thicknesses of the active layers, wavelength-tunable DFB lasers were achieved. As shown in Fig. 7c, various lasing spectra were obtained across from 442 nm to 505 nm. For SF-PyF, by simply regulating various film thicknesses (from 123 nm to 203 nm) and grating periods (280 nm, 290 nm, 300 nm), 5 lasing spectra were obtained with a spectral window of 30 nm (from 442 nm to 472 nm). With the same method, another 5 lasing spectra for Py-PyF were recorded with a spectral window of 29 nm (from 476 nm to 505 nm).

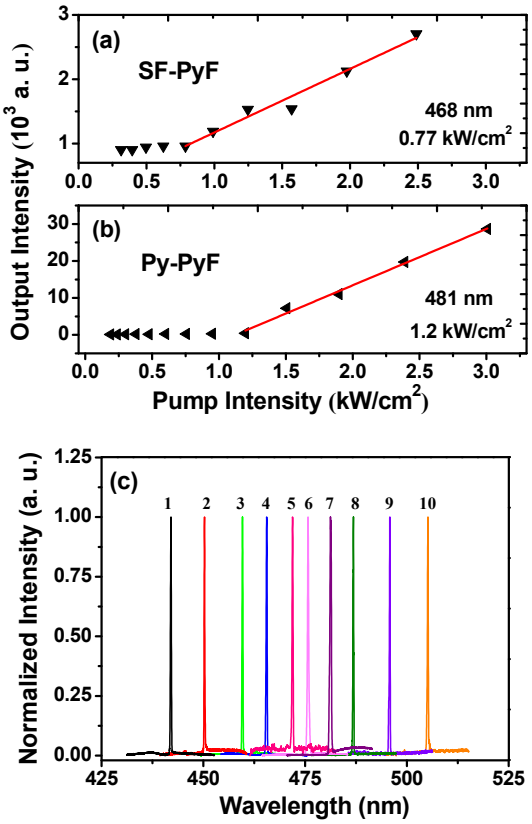

Fig. 7 Output intensity versus the pump intensity for (a) SF-PyF and (b) Py-PyF. (c) Lasing spectra based on various DFB resonators for SF-PyF films (1-5) and Py-PyF films (6-10) at different thicknesses: 123 nm with Λ = 280 nm for λ = 442 nm (1), 150 nm with Λ = 280 nm for λ = 450 nm (2), 150 nm with Λ = 300 nm for λ = 460 nm (3), 123 nm with Λ =290 nm for λ = 465 nm (4), 203 nm with Λ = 300 nm for λ = 472 nm (5), 96 nm with Λ = 280 nm for λ = 476 nm (6), 96 nm with Λ = 290 nm for λ = 481 nm (7), 127 nm with Λ = 290 nm for λ = 487 nm (8), 176 nm with Λ = 290 nm for λ = 496 nm (9), 230 nm with Λ = 300 nm for λ = 505 nm (10).

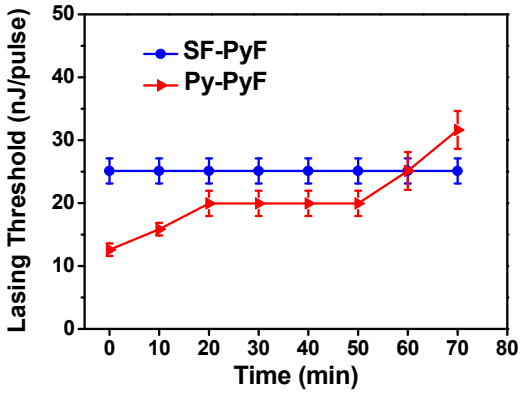

Fig. 8 Lasing threshold of the DFB lasers as a function of the processing time under water conditions (80 °C).

Lasing stability.

In order to evaluate the device reliability, the DFB lasers were immersed in water (80 °C) and assessed by monitoring the lasing threshold as a function of the processing time following excitation at 355 nm. As shown in Fig. 8, both lasers exhibited good water-oxygen stability. The lasing threshold of Py-PyF laser slightly increased by 1.7 fold (from 12.6 nJ/pulse to 20 nJ/pulse) after 50 min, and 2.5 fold (from 12.6 nJ/pulse to 32 nJ/pulse) after 70 min, which still maintained at a relatively low level. In addition, the lasing peak as well as the linewidth remained stable (490 nm, 0.4 nm), which revealed the high spectral stability of Py-PyF laser in water despite the slightly increased lasing threshold. For SF-PyF laser, the lasing threshold maintained almost the same (25.1 nJ/pulse, up to 70 min in hot water). Besides the stability of lasing threshold, the lasing peak and the linewidth kept the same (449 nm, 0.28 nm), suggesting the extremely high spectral and optical gain stability. Consequently, the invariance of the lasing threshold, the lasing peak and the linewidth further confirmed the outstanding environmental stability of SF-PyF laser. The results suggested that highly stable lasing properties were close related to the novel molecular design for the pyrene-capped spirofluorene-centered starburst sample.

View Article Online
DOI: 10.1039/C6TC01606E

Conclusions

In conclusion, a novel set of pyrene-capped starburst orgainc emitters (SF-PyF and Py-PyF) have been successfully designed, synthesized, and explored as gain media for OSLs. The resulting molecules, especially SF-PyF, exhibited outstanding high photostability in ambient atmosphere. Upon annealing at 240 °C, the ASE threshold for SF-PyF increased by 2.3 fold with unchanged ASE spectra. Additionally, the ASE actions was still detectable with further increasing annealing temperature (up to 300 °C). The 1D DFB lasers based on the samples were fabricated with low thresholds of 0.77 kW/cm^2 for SF-PyF and 1.2 kW/cm^2 for Py-PyF. By selecting proper grating periods and film thicknesses, the lasing peaks could be facilely tuned from 442 nm to 472 nm for SF-PyF and 476 nm to 505 nm for Py-PyF, respectively. It is worthwhile to mention that the DFB lasers based on the samples have shown impressive ambient stability under water condition. The excellent stability of ASE spectra, electroluminescence spectra and lasing spectra under harsh conditions manifests that the resulting pyrene-capped starburst emitters are beneficial for improving the lasing stability issues. The study sheds light on exploring robust organic gain media toward electrically-pumped OSLs.

Acknowledgements

We acknowledge financial support of the National Key Basic Research Program of China (973 Program, 2014CB648300), the National Natural Science Foundation of China (21422402, 20904024, 51173081, 61136003), the Natural Science Foundation of Jiangsu Province (BK20140060, BK20130037, BM2012010), Program for Jiangsu Specially-Appointed Professors (RK030STP15001), Program for New Century Excellent Talents in University (NCET-13-0872), Specialized Research Fund for the Doctoral Program of Higher Education (20133223110008, and 20113223110005), the Synergetic Innovation Center for Organic Electronics and Information Displays, the Priority Academic Program Development of Jiangsu Higher Education Institutions (PAPD), the NUPT "1311 Project", the Six Talent Plan (2012XCL035), the 333 Project (BRA2015374) and the Qing Lan Project of Jiangsu Province.

Notes and references

1 L. H. Xie, C. R. Yin, W.-Y. Lai, Q. L. Fan and W. Huang, *Prog. Polym. Sci.,* 2012, **37**, 1192.
2 P. M. Beaujuge and J. M. J. Fréchet, *J. Am. Chem. Soc.,* 2011, **133**, 20009.
3 A. L. Kanibolotsky, I. F. Perepichkaz and P. J. Skabara, *Chem. Soc. Rev.,* 2010, **39**, 2695.
4 T. P. I. Saragi, T. Spehr, A. Siebert, T. Fuhrmann-Lieker and J. Salbeck, *Chem. Rev.,* 2007, **107**, 1011.
5 I. D. W. Samuel and G. A. Turnbull, *Chem. Rev.,* 2007, **107**, 1272.
6 G. D. Scholes and G. Rumbles, *Nat. Mater.,* 2006, **5**, 683.
7 C. Grivas and M. Pollnau, *Laser & Photonics Rev.,* 2012, **6**, 419.
8 W.-Y. Lai, R. D. Xia, Q. Y. He, P. A. Levermore, W. Huang and D. D. C. Bradley, *Adv. Mater.,* 2009, **21**, 355.
9 F. Hide, M. A. García, B. J. Schwartz, M. R. Andersson, Q. B. Pei and A. J. Heeger, *Science,* 1996, **273**, 1833.
10 S. Chénais and S. Forget, *Polym Int.,* 2012, **61**, 390.
11 S. Z. Bisri, T. Takenobu and Y. Iwasa, *J. Mater. Chem. C,* 2014, **2**, 2827.
12 H. Kim, N. Schulte, G. Zhou, K. Müllen and F. Laquai, *Adv. Mater.,* 2011, **23**, 894.
13 B. K. Yap, R. D. Xia, M. Campoy-quiles, P. N. Stavrinou and D. D. C. Bradley, *Nat. Mater.,* 2008, **7**, 376.
14 C. Rothe, F. Galbrecht, U. Scherf and A. Monkman, *Adv. Mater.,* 2006, **18**, 2137.
15 J. Y. Li, F. Laquai and G. Wegner, *Chem. Phys. Lett.,* 2009, **478**, 37.
16 F. Liu, W.-Y. Lai, C. Tang, H. B. Wu, Q. Q. Chen, B. Peng, W. Wei, W. Huang and Y. Cao, *Macromol. Rapid Commun.,* 2008, **29**, 659.
17 M. Sang, S. Cao, J. Yi, J. Huang, W.-Y. Lai and W. Huang, *RSC Adv.*, 2016, **6**, 6266.
18 J. Yi, J. Huang, Y. Lin, C.-F. Liu, T. Cheng, Y. Jiang, W. Tang, W.-Y. Lai and W. Huang, *RSC Adv.*, 2016, **6**, 49903.
19 S. L. McFarlane, L. S. Coumont, D. G. Piercey, R. McDonald and J. G. C. Veinot, *Macromolecules,* 2008, **41**, 7780.
20 C. F. Liu, Y. Jiu, J. Wang, J. Yi, X. W. Zhang, W. Y. Lai and W. Huang, *Macromolecules*, 2016, **49**, 2549.
21 G. Tsiminis, N. A. Montgomery, A. L. Kanibolotsky, A. Ruseckas, I. F. Perepichka, P. J. Skabara, G. A. Turnbull and I. D. W. Samuel, *Semicond. Sci. Technol.,* 2012, **27**, 094005.
22 W. D. Xu, J. P. Yi, W.-Y. Lai, L. Zhao, Q. Zhang, W. Hu, X.-W. Zhang, Y. Jiang, L. Liu and W. Huang, *Adv. Funct. Mater.,* 2015, **25**, 4617.
23 T. M. Figueira-Duarte and K. Müllen, *Chem. Rev.,* 2010, **111**, 7260.
24 E. B. Namdas, M. H. Tong, P. Ledochowitsch, S. R. Mednick, J. D. Yuen, D. Moses and A. J. Heeger, *Adv. Mater.,* 2009, **21**, 799.

View Article Online
DOI: 10.1039/C6TC01606E

Graphic Abstract

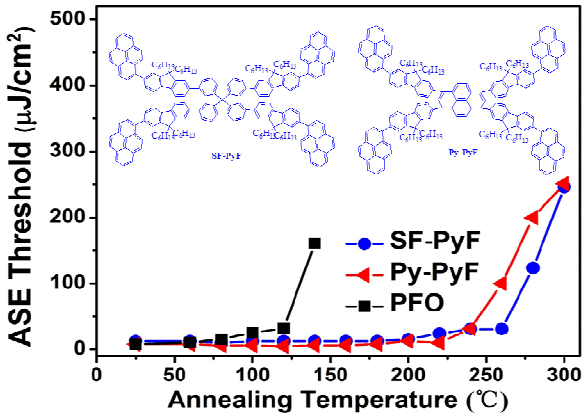

A novel set of pyrene-capped starburst orgainc emitters have been designed, synthesized and explored as efficient emitters for organic lasers.